Journal of Hazardous Materials 422 (2022) 126916

Contents lists available at ScienceDirect

Journal of Hazardous Materials

journal homepage: www.elsevier.com/locate/jhazmat

Co-removal of 2,4-dichlorophenol and nitrate using a palladized biofilm: Denitrification-promoted microbial mineralization following catalytic dechlorination

Chengyang Wu [a,b], Luman Zhou [a,b], Chen Zhou [c], Yun Zhou [d], Siqing Xia [a,b,*], Bruce E. Rittmann [c]

[a] State Key Laboratory of Pollution Control and Resource Reuse, College of Environmental Science and Engineering, Tongji University, Shanghai, China
[b] Shanghai Institute of Pollution Control and Ecological Security, Shanghai, China
[c] Biodesign Swette Center for Environmental Biotechnology, Arizona State University, Tempe, AZ, USA
[d] Huazhong Agricultural University, Wuhan, China

ARTICLE INFO

Editor: Dr. C. Ling Xin

Keywords:
Membrane biofilm reactor
Palladium nanoparticle
Hydrodechlorination
Microbial mineralization
Denitrification

ABSTRACT

The effects of nitrate on 2,4-dichlorophenol (2,4-DCP) dechlorination and biodegradation in a hydrogen (H_2)-based palladized membrane biofilm reactor (Pd-MBfR) were studied. The Pd-MBfR was created by synthesizing palladium nanoparticle (Pd^0NPs) that spontaneously associated with the biofilm to form a Pd^0-biofilm. Without input of nitrate, the Pd-MBfR had rapid and stable catalytic hydrodechlorination: 93% of the 100-μM influent 2,4-DCP was continuously converted to phenol, part of which was then fermented via acetogenesis and methanogenesis. Introduction of nitrate enabled phenol mineralization via denitrification with only a minor decrease in catalytic hydrodechlorination. Phenol-degrading bacteria capable of nitrate respiration were enriched in the Pd^0-biofilm, which was dominated by the heterotrophic genera *Thauera* and *Azospira*. Because the heterotrophic denitrifiers had greater yields than autotrophic denitrifiers, phenol was a more favorable electron donor than H_2 for denitrification. This feature facilitated phenol mineralization and ameliorated denitrification inhibition of catalytic dechlorination through competition for H_2. Increased nitrite loading eventually led to deterioration of the dechlorination flux and selectivity toward phenol. This study documents simultaneous removal of 2,4-DCP and nitrate in the Pd-MBfR and interactions between the two reductions.

1. Introduction

Chlorophenols (CPs) are produced in large quantities and frequently detected in natural environments (Estevinho et al., 2007; Gonzalez et al., 2012; Büchel, 1984). 2,4-dichlorophenol (2,4-DCP) that heavily used in herbicides production and preservatives is one of the most abundant CPs in aquatic environments (House et al., 1997; Gao et al., 2008). It is also a disinfection by-product (DBP) that is more toxic that the common aliphatic DBPs (e.g., trihalomethanes and haloacetic acids) (Liu et al., 2020; Liu and Zhang, 2014). 2,4-DCP has been detected at ppm levels in drinking water (Tang and Huang, 1996; Zhang et al., 2005) and is listed as a priority pollutant by the U.S. Environmental Protection Agency (EPA) due to its toxicity to ecological and human health; the EPA set a maximum contaminant level (MCL) in drinking waters of 0.1 mg L^{-1} (United States Environmental Protection Agency, 2012). Nitrate (NO_3^-) is a frequent co-contaminant with 2,4-DCP in surface water or groundwater (Yang et al., 2021) and can induce methemoglobinemia in infants and accelerate eutrophication (Addiscott and Benjamin, 2004).

Coupled biological reductions of 2,4-DCP and NO_3^- involve initial reductive dechlorination of 2,4-DCP followed by mineralization of dechlorinated metabolites via denitrification (Addiscott and Benjamin, 2004; Long et al., 2018; Wang et al., 2013). However, biodegradation of CPs is hampered by the need for long acclimation and solids-retention times. Furthermore, dechlorination of *para*-Cl is intrinsically difficult (Long et al., 2020) and can lead to accumulation of *para*-chlorophenol (4-CP), which is toxic and can inhibit the range of dechlorination and mineralization reactions (Yang et al., 2021; Li et al., 2010).

An alternative to biodegradation of CPs is palladium (Pd)-based hydrodechlorination (Chaplin et al., 2012), in which hydrogen gas (H_2) is the sole energy and chemical input and the end-product is phenol,

* Corresponding author at: State Key Laboratory of Pollution Control and Resource Reuse, College of Environmental Science and Engineering, Tongji University, Shanghai, China.
E-mail addresses: siqingxia@gmail.com, siqingxia@tongji.edu.cn (S. Xia).

https://doi.org/10.1016/j.jhazmat.2021.126916
Received 28 June 2021; Received in revised form 2 August 2021; Accepted 14 August 2021
Available online 18 August 2021

Table 1
MBfR parameters for operations and average performance at steady state for all stages.

Stage	2,4-DCP						NO_3^-					Duration	Recirculation rate
	In (μM)	Out	Surface loading (mmol m^{-2} d^{-1})	flux	Electron donor consumed (e^--meq m^{-2} d^{-1})		In (μM)	Out	Surface loading (mmol m^{-2} d^{-1})	flux	Electron donor consumed (e^--meq m^{-2} d^{-1})	(day)	(mL min^{-1})
S0[a]	–	–	–	–	–	–	700	85.7	99	86.3	431	[a]	150
S1a	50	5.1	6.7	6.4	22.5		–	–	–	–	–	1–10	150
S1b	100	6.9	13.5	12.5	49.3		–	–	–	–	–	11–70	150
S1c	100	16.1	13.4	11.1	39.1		–	–	–	–	–	71–90	50
S2	100	5.7	13.7	12.9	46.0		100	0	14.5	14.5	72.6	91–111	150
S3	100	6.1	13.7	12.9	47.7		300	0	45.0	45.0	225	112–134	150
S4	100	13.7	14.0	12.0	42.8		600	0	84.7	84.7	459	135–160	150

[a] S0 denotes the operation of the denitrifying MBfR before deposition of Pd^0. Stage 0 was for accumulation of a denitrifying biofilm and lasted for 63 days. The reactor was a Pd-MBfR for Stages 1 through 4.

which is readily biodegradable. Despite its advantages, Pd-based hydrodechlorination by conventional catalytic approaches has been thwarted by three challenges: poor efficiency of the H_2 supply (Zhou et al., 2019), catalyst deactivation due to its loss (Cantillo and Kappe, 2014; Greco et al., 2015), and the need for down-stream removal of end-products before discharge (Long et al., 2020; Wu et al., 2021).

The H_2-based membrane biofilm reactor (MBfR) efficiently delivers H_2 to a biofilm by its diffusion through the walls of hollow-fiber membranes in a bubble-free manner that can be controlled by the H_2 pressure (Lee and Rittmann, 2002). The MBfR achieved microbially driven Pd recovery, and the *in-situ* generated palladium nanoparticle (Pd^0NPs) spontaneously associated with the biofilm (Pd^0-biofilm), which effectively immobilized and stabilized them in a form that catalyzed hydrodechlorination (Zhou et al., 2016b, 2017). In addition, biofilms enabled NO_3^- respiration using phenol as the electron donor (Long et al., 2020; Xia et al., 2011). These features of a palladized MBfR ought to overcome all the challenges of conventional catalyst approaches.

By coupling a biofilm and *in-situ* generated Pd^0NPs in a H_2-MBfR, we created a synergistic system: a palladized MBfR, or Pd-MBfR. While simultaneous reduction of CPs and NO_3^- by a Pd-MBfR has been documented (Long et al., 2021), interactions between two reductions remain unaddressed.

One possible interaction is that denitrification of NO_3^- or NO_2^- inhibits catalytic dechlorination by competing for H_2. Furthermore, catalytic NO_2^- reduction can compete directly with catalytic dechlorination of 2,4-DCP. Therefore, one objective of this study is to test the effects of NO_3^- on catalytic dechlorination of 2,4-DCP in a Pd-MBfR.

A second interaction stems from the fact that phenol can be mineralized by bacteria carrying out denitrification (Long et al., 2018, 2020). Thus, catalytic reduction of 2,4-DCP to phenol generates a second electron donor that can increase the rate of denitrification as phenol is mineralized. A second objective is to evaluate phenol mineralization via denitrification. In particular, is phenol a more favorable electron donor than H_2? However, it is possible that catalytic reduction of NO_2^- to N_2 will inhibit denitrification and phenol mineralization (Zhou et al., 2017).

We evaluated the interactions by measuring the kinetics of 2,4-DCP reductive dechlorination, phenol mineralization, and NO_3^- reduction, along with changes in the microbial community's structure and function.

2. Materials and methods

2.1. MBfR configuration

We operated an MBfR that shared the same dual-tube configuration (illustrated in Fig. S1, Supporting Information) as in a previous work (Wu et al., 2021). The reactor contained a main bundle of 32 nonporous polypropylene hollow-fiber membranes (200-μm outer diameter, 100–110-μm inner diameter, Teijin, Japan) in one column and another bundle of 10 identical fibers used as sampling coupons in the other column. The reactor had a 65-mL working volume and a total membrane surface area of 54 cm^2. Pure H_2 gas was constantly supplied to the fiber bundles, with pressures adjusted by a gas regulator, and it diffused through the fiber walls in a bubble-free manner. The liquid of the reactor was well mixed by a recirculation rate of 150 mL min^{-1} provided by a peristaltic pump (Longer 1515X, China). Thus, the solute concentrations inside the reactor were equal to its effluent concentrations. The temperature was maintained at 25 ± 2 °C.

2.2. Inoculation, feeding, and start up for the MBfR

We inoculated the MBfR with 10-mL anoxic sludge from the Wusong wastewater treatment plant (Baoshan, Shanghai) and allowed a biofilm to form by recirculating a mineral salt medium (described in Table S1, Supporting Information) containing 1-mM NO_3^- for 48 h; the H_2 pressure was 20 psig (2.4 atm absolute). After the batch period, we fed the reactor continuously with a 0.7-mM NO_3^- (10 mg N L^{-1}) medium to accumulate biofilm on the membranes; the flow rate was constant at 0.53 mL min^{-1} (or a hydraulic retention time (HRT) of 2 h), and the H_2 pressure was 20 psig; this was Stage 0. The influent medium was stored in a 2.5-L glass bottle that had been sparged for 15 min with pure N_2 gas to eliminate dissolved oxygen. After 63 days of operation, NO_3^- removal was consistently 85–90% (Fig. S2), and a mature biofilm had formed on the fiber surfaces.

2.3. Synthesis of biogenic Pd^0NPs supported on biofilm

After the mature biofilm was formed, we introduced medium containing Pd(II) (0.8-mM Na_2PdCl_4) in a 2-mM phosphate buffer (pH 7.2) into the MBfR. After this medium was added, the MBfR was run in batch mode with the H_2 pressure of 20 psig to produce biogenic Pd^0NPs within the biofilm (creating a Pd-MBfR) through enzymatic and autocatalytic reductions (Zhou et al., 2016a). The Pd(II) concentration in the medium was analyzed by inductively coupled plasma optical emission spectrometer (ICP-OES; Agilent 720ES, USA). The Pd^0NPs-deposition process was carried out three times (each batch lasted 2 days) until a dark Pd^0-biofilm formed on the fibers, and more than 99% of the input soluble Pd(II) was reduced after each addition of Pd(II). The palladized biofilm contained 32.8 mg Pd^0.

2.4. Long-term continuous operation of the Pd-MBfR

Continuous operation in the Pd-MBfR was divided into four stages that had an influent flow rate of 0.53 mL min^{-1} and H_2 pressure of 20 psig. Table 1 summarizes conditions in all stages. The influent 2,4-DCP concentration was 50 μM in Stage 1a and 100 μM during Stages 1b and 1c. The recirculation rate was decreased from 150 to 50 mL min^{-1} for Stage 1c. To evaluate the effect of NO_3^- on 2,4-DCP removal, we then kept the influent 2,4-DCP at 100 μM and applied NO_3^- in the influent at

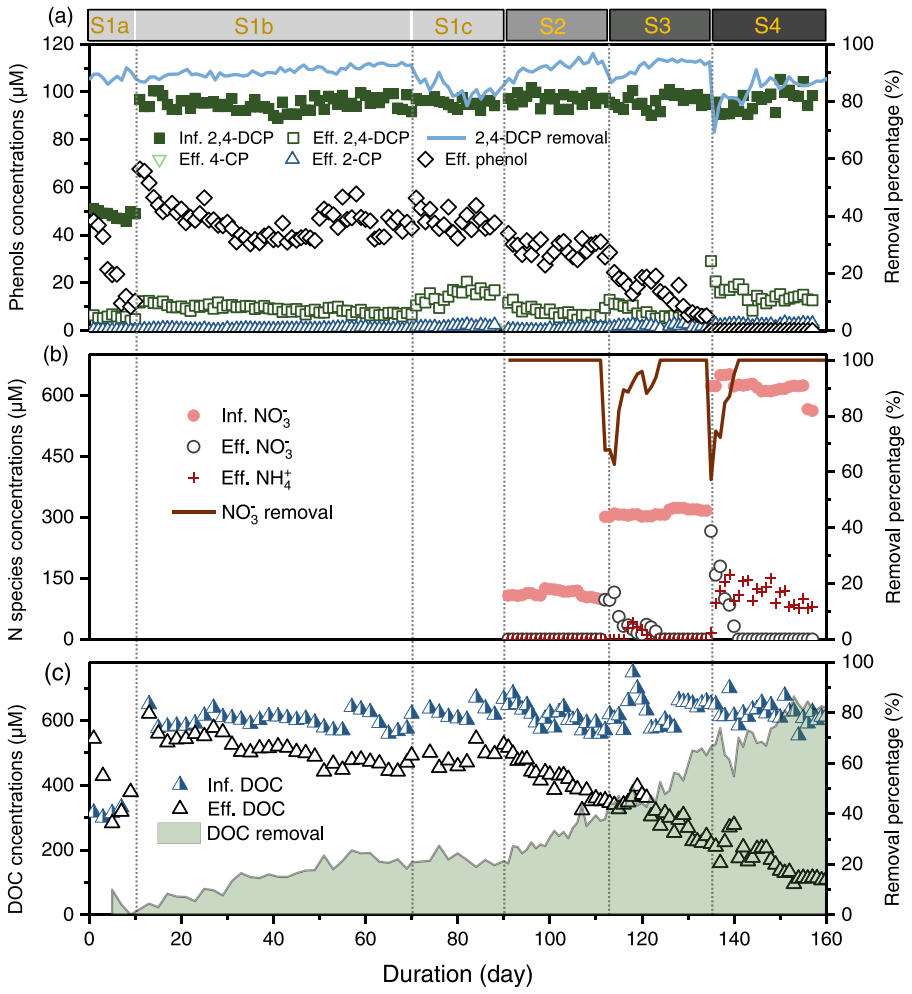

Fig. 1. Results for continuous operation in the Pd-MBfR with a flow rate of 0.53 mL min^{-1} and supplied with 20 psig H_2 (2.4 atm absolute). The dashed vertical lines denote stage shifts. NO_2^- was not detected throughout the 160 days and the effluent 4-CP was negligible (< 1 μM).

100, 300, and 600 μM through Stages 2, 3, and 4, respectively. The influent was prepared by adding a 5-mM 2,4-DCP stock solution to the deoxygenated water containing basic medium that had been purged with N_2 (Table S1). The stock solution was prepared by dissolving 2,4-DCP in deoxygenated water and could not be purged with an inert gas due to the volatility of 2,4-DCP, and this led to a dissolved oxygen (DO) concentration in the influent medium of 0.8–1.1 mg L^{-1}. DO in the Pd-MBfR effluent was < 0.1 mg L^{-1}. In each stage, the reactor was considered at steady state when the effluent concentration of all the substrates and the products had ≤ 5% variation for at least 3 HRTs.

2.5. Dechlorination experiments for evaluating the nitrite effect

We explored the effect of NO_2^- reduction on catalytic dechlorination after completion of the long-term experiments. This series were divided into 5 substages in which NO_3^- was removed from influent, and influent NO_2^- concentrations were set at 0, 150, 250, 500, or 750 μM. Each substage lasted 8 HRTs, long enough for the system to reach steady state for the liquid phase. Replicate samples were collected at 6, 7, and 8 HRTs, and the results were presented as the average values ± the standard deviation.

2.6. Sample collection and characterization

To examine the fate of Pd^0NPs associated with the biofilm, we sampled the Pd-MBfR's biofilm by cutting off an ~5 cm-long fiber at the end of Pd^0NP synthesis (day 0) and day 90. After chemical fixation and ultra-microtome slicing, these fibers were characterized using transmission electron microscopy (TEM, Hitachi H-7650, Japan) and high-resolution electron microscopy (HRTEM, FEI F20, The Netherlands) coupled with energy-dispersive X-ray spectroscopy (EDX). In addition, we scratched Pd^0-biofilm solids off the fibers and then immediately freeze-dried them for subsequent X-ray diffraction (XRD), X-ray photoelectron spectrum (XPS), and Fourier transform infrared spectroscopy (FTIR) analyses. Detailed information on these analyses is in published works (Wu et al., 2021; Long et al., 2017).

2.7. DNA extraction and microbial community analyses

At the end of each stage, we cut off a 10-cm section from a coupon fiber in the reactor and then tied the end of the remaining fiber. We followed the procedures of biofilm separation and DNA extraction described by Xia et al. (2016). We used the barcoded primer set 338F/806R to amplify the conserved V3-V4 regions of the bacterial 16S rRNA gene and purified the PCR products using the DNA Gel Extraction Kit (Axygen Biosciences, USA). The amplicons were sent to Majorbio Technology (Shanghai, China) to process Illumina MiSeq sequencing with standard protocols. We processed the raw data using QIIME 1.9.1 suite (Caporaso et al., 2010), as described in detail in Supporting Information.

We then used the Phylogenetic Investigation of Communities by Reconstruction of Unobserved States (PICRUSt) pipeline to predict the

metagenomic compositions of the biofilms communities based on 16S rRNA gene-data and using the latest Kyoto Encyclopedia of Genes and Genomes (KEGG) database (Langille et al., 2013; Xie et al., 2011).

2.8. Sampling and analyses

Liquid samples from the reactors were collected at preselected time intervals and immediately filtered through 0.22-μm polytetrafluoroethylene syringe filters. We measured the filtered samples for 2,4-DCP, *ortho*-chlorophenol (2-CP), 4-CP, phenol, and 4-hydroxybenzoate using a high-performance liquid chromatography (HPLC, Shimadzu LC-20A, Japan). Cl^-, NO_2^-, and NO_3^- were quantified by an ion chromatograph (IC, Dionex Aquion, USA). Ammonium nitrogen (NH_4^+-N) was measured using Nessler's reagent colorimetric method according to Standard Methods (HJ 535-2009, China). Dissolved organic carbon (DOC) was determined by a total organic carbon analyzer (Shimadzu TOC-L, Japan). A gas chromatograph (Agilent 6890A, USA) with a flame ionization detector (FID) was employed to assess acetate. Methane in the headspace of the reactor was assessed by a gas chromatograph (Agilent 6890A, USA) equipped with a thermal conductivity detector (TCD), and we computed the aqueous concentrations using Henry's constants (4.18×10^6 kPa). We also collected unfiltered samples and digested them using thick hot mixture of hydrochloric acid and nitric acid to dissolve any solid Pd. The filtered and unfiltered samples were assayed for the concentrations of soluble and total Pd, respectively, using an inductively coupled plasma mass spectrometry (ICP-MS; Thermo 7700, USA). The concentration of solid Pd was calculated by subtracting soluble Pd from total Pd in the effluent. pH and DO were measured using a multi-Parameter Meter (HACH HQ40d, USA). The detection limits of the analytes are summarized in Table S2.

2.9. Calculations

The surface loading rates (*SLR*, mmol m^{-2} d^{-1}) and the removal fluxes (*J*, mmol m^{-2} d^{-1}) of substrates were calculated by

$$SLR = \frac{C_0 \cdot Q}{A} \tag{1}$$

$$J = \frac{(C_0 - C_e) \cdot Q}{A} \tag{2}$$

where C_0 and C_e are 2,4-DCP concentration in the influent and effluent (mmol m^{-3}), respectively; Q is the influent flow rate (m^3 d^{-1}); and A is the membrane surface area (m^2). The dechlorination flux in electron equivalents (e^--meq m^{-2} d^{-1}) was calculated based on released Cl^- concentrations according to reaction stoichiometry:

$$2,4-\mathrm{DCP} + 4e^- + 2H^+ \rightarrow \mathrm{phenol} + 2Cl^- \tag{3}$$

The NO_3^- flux in electron equivalents (e^--meq m^{-2} d^{-1}) was calculated from

$$NO_3^- + 5e^- + 6H^+ \rightarrow 0.5N_2 + 3H_2O \tag{4}$$

To indicate if the H_2 supply was limiting, the maximum H_2-supply flux at applied H_2 pressure of 20 psig (i.e., 490 e^--meq m^{-2} d^{-1}) was calculated according to Tang et al. (2012).

3. Results and discussion

3.1. Continuous co-removal of 2,4-DCP and NO_3^-

3.1.1. Phenol fermentation following catalytic dechlorination of 2,4-DCP

Fig. 1 presents the concentrations of 2,4-DCP, 2-CP, 4-CP, phenol, NO_3^-, NH_4^+, and DOC in the Pd-MBfR effluent during continuous operation. For Stage 1a, the Pd-MBfR showed immediate removal of 2,4-DCP: Over 90% of the 50 μM influent 2,4-DCP was removed, and no 2-CP or 4-CP accumulated. With a doubled influent concentration in Stage 1b, the 2,4-DCP flux almost proportionally increased, from 6.4 to 12.5 mmol m^{-2} d^{-1} (Table 1), bringing about stable 2,4-DCP removal of 92.8 ± 0.4%. Phenol was the major dechlorination product (~99% selectivity), with monochlorphenols (MCPs, i.e., 2-CP and 4-CP) < 1%. In Stage 1c, when the recirculation rate was decreased, the removal of 2,4-DCP dropped to 83.0 ± 1.3%, while selectivity toward 2-CP and 4-CP increased to 2.3% and 0.8%, respectively. The lower circulation velocity increased the liquid diffusion layer thickness, introducing more resistance to CPs transfer from the bulk to the biofilm surface (Rittmann and McCarty, 2020). Fig. S3 documents that Cl^- was produced stoichiometrically from 2,4-DCP dechlorination. The good closure of the Cl mass balance – an average 93% recovery of Cl from the removed 2,4-DCP – confirms that 2,4-DCP was removed via catalytic dechlorination.

In Stages 1b and 1c, the input DO was only about 4% of that needed to completely mineralize phenol produced from 2,4-DCP, and only ~20% of the input 2,4-DCP was mineralized to inorganic carbon at steady state (i.e., ~20% DOC loss, Fig. 1c). With incomplete mineralization, three metabolites of phenol biodegradation were detected in the effluent: 4-hydroxybenzoate, acetate, and methane (Fig. S4). Anaerobic biodegradation of phenol via 4-hydroxybenzoate and benzoate and finally to acetate and methane has been widely reported (Qiu et al., 2008; Weigel et al., 1990; Holmes et al., 2012):

$$C_6H_6O + 5H_2O \rightarrow 3CH_3COOH + 2H_2 \tag{5}$$

$$CH_3COOH \rightarrow CH_4 + CO_2 \tag{6}$$

The overall reaction is

$$C_6H_6O + 5H_2O \rightarrow 3CH_4 + 3CO_2 + 2H_2 \quad \Delta G^{0'} = -100.6\ \mathrm{kJ \cdot mol^{-1}phenol} \tag{7}$$

Thermodynamically, phenol transformation to CH_4, CO_2, and H_2 is feasible.

The measured phenol depletion (~42 μM loss, Fig. 1a) and inorganic carbon formation (118 ± 9 μM, Fig. 1c) were approximately equivalent to the stoichiometry of Eq. (7). Taken together, the stoichiometric results and the detected metabolites support that phenol was transformed initially via the benzoate-CoA pathway, which generated H_2, CH_4, and CO_2 (Weigel et al., 1990; Holmes et al., 2012; Zhang et al., 2013).

3.1.2. The effect of NO_3^- on catalytic dechlorination and biodegradation of 2,4-DCP

Introducing NO_3^- in Stages 2–4 led to three clear trends (Fig. 1b and c). First, higher NO_3^- loadings significantly promoted DOC removal, up to 82.1 ± 2.5% by the end of Stage 4. The removal of DOC was proportional to depletion of NO_3^-, which reinforces that mineralization of phenol was enabled by the input of NO_3^- as a microbial electron acceptor. Second, NO_3^- was microbially denitrified to NO_2^- using phenol as electron donor in all stages, because Pd^0NPs are not able to catalyze NO_3^- reduction to NO_2^- without a modifying promotor such as Cu, Sn, or In (Al Bahri et al., 2013). NO_2^- reduction could have been shared by microbial denitrification and Pd-catalyzed reduction (Zhou et al., 2016a). Third, modest NO_3^- loading (Stages 2 and 3) had no influence on dechlorination, while the highest NO_3^- loading (Stage 4) decreased 2,4-DCP removal from 93% to 86%. This trend likely was due to competition for electrons from H_2 among reductions of 2,4-DCP, NO_3^-, and NO_2^-.

The stoichiometry of phenol mineralization via full denitrification of NO_3^- is

$$C_6H_6O + 5.6NO_3^- \rightarrow 6CO_2 + 2.8N_2 + 5.6OH^- + 0.2H_2O \tag{8}$$

when biomass synthesis is ignored. However, the calculated f_s value (the portion of the electrons converted to biomass) indicates that biomass synthesis can require as much as 65% of total demand for electron donor

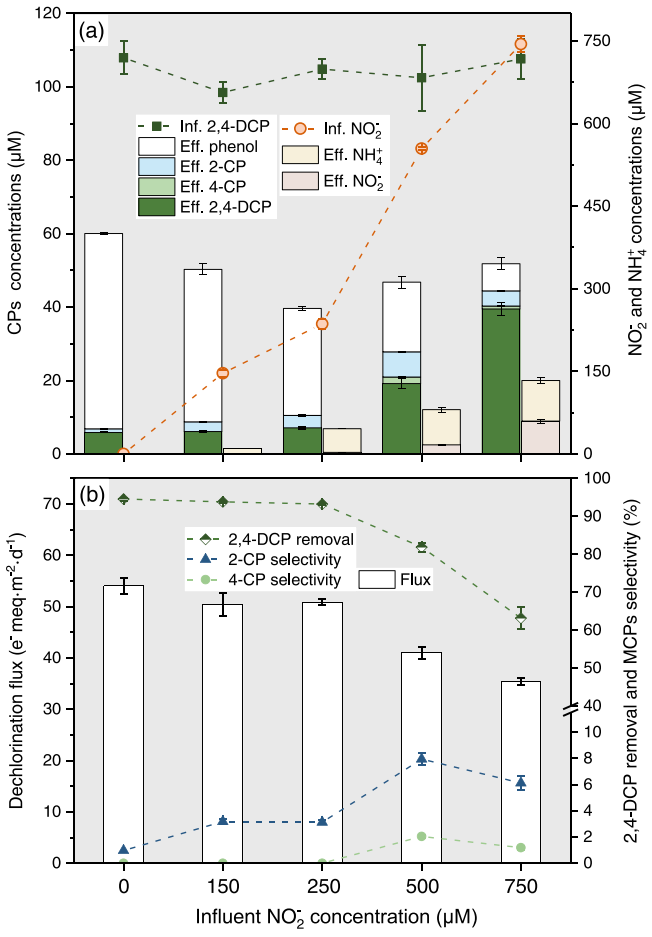

Fig. 2. Effects of NO_2^- loading on dechlorination rate and product selectivity for the Pd-MBfR.

(Rittmann and McCarty, 2020). When considering biomass synthesis, the reaction stoichiometry is

$$C_6H_6O + 2.61NO_3^- + 2.61H^+ \rightarrow 2.75CO_2 + 0.98N_2 + 0.65C_5H_7O_2N + 2.01H_2O \quad (9)$$

Thus, complete oxidation of the 100 μM phenol (from 100 μM 2,4-DCP) could have consumed from 260 to 560 μM NO_3^-.

In Stage 3, the influent NO_3^- of 300 μM was within this range for microbial mineralization of phenol generated from 2,4-DCP dechlorination. However, the observed DOC removal of 67.5 ± 1.3% was lower than 2,4-DCP removal (93%), which can be explained by two phenomena. Firstly, some of the DOC was soluble microbial products (SMP) generated by the biomass (Rittmann and McCarty, 2020; Laspidou and Rittmann, 2002). Secondly, some NO_2^- reduction used H_2 as the electron donor, not phenol or its downstream metabolites.

In Stage 4, influent NO_3^- of 600 μM was more than sufficient for phenol mineralization. Phenol removal was nearly complete, and DOC removal was close to the 2,4-DCP removal; thus, phenol was almost completely mineralized. NO_2^- was reduced to a significant degree by Pd^0 catalysis. This is verified by the accumulation of NH_4^+ (~70–150 μM) in Stage 4, since NH_4^+ is a product of Pd-catalyzed NO_2^- reduction (Zhou et al., 2017; Shin et al., 2014). With Pd^0 catalysis alone, selectivity to NH_4^+ (over N_2) is favored by a higher H_2/N ratio, but the Pd-MBfR had a combination of microbiological denitrification and Pd^0 catalysis of NO_2^-. Increased input of NO_3^- shifted the balance away from microbial denitrification of NO_2^- (Zhou et al., 2017), which allowed catalytic reduction of NO_2^- to NH_4^+ to become evident. It is possible that catalytic NO_2^- reduction in Stage 4 was responsible for the small inhibition of dechlorination of 2,4-DCP. These results demonstrate the requirement for stoichiometric inputs of NO_3^- to enable complete phenol mineralization with a minor sacrifice of dechlorination performance.

3.1.3. *Higher NO_2^- loading lowered the dechlorination flux and selectivity to phenol*

Because a high loading of NO_3^- slightly lowered 2,4-DCP removal, probably due to competition between 2,4-DCP and NO_2^- reductions via catalysis, we directly investigated the competitive effect of NO_2^- reduction on 2,4-DCP dechlorination in Pd-MBfR experiments in which NO_2^- replaced NO_3^- in the influent. Fig. 2 shows moderate NO_2^- loading (250 μM, or 3.5 mg N L^{-1}) resulted in a slight decrease of dechlorination flux (from 54.1 to 50.8 e^--meq m^{-2} d^{-1}) and a small MCPs accumulation (3.1% selectivity), since NO_2^- was completely removed. Higher NO_2^- loadings (≥ 500 μM) led to an obvious decrease of the dechlorination flux (from 54.1 to 35.3 e^--meq m^{-2} d^{-1}), greater selectivity to MCPs (~10%), and residual NO_2^- in the effluent (~60 mM). The most likely cause was increased desorption of CPs due to competition with NO_2^- for adsorption sites, since the H_2 supply was not limited. According to their

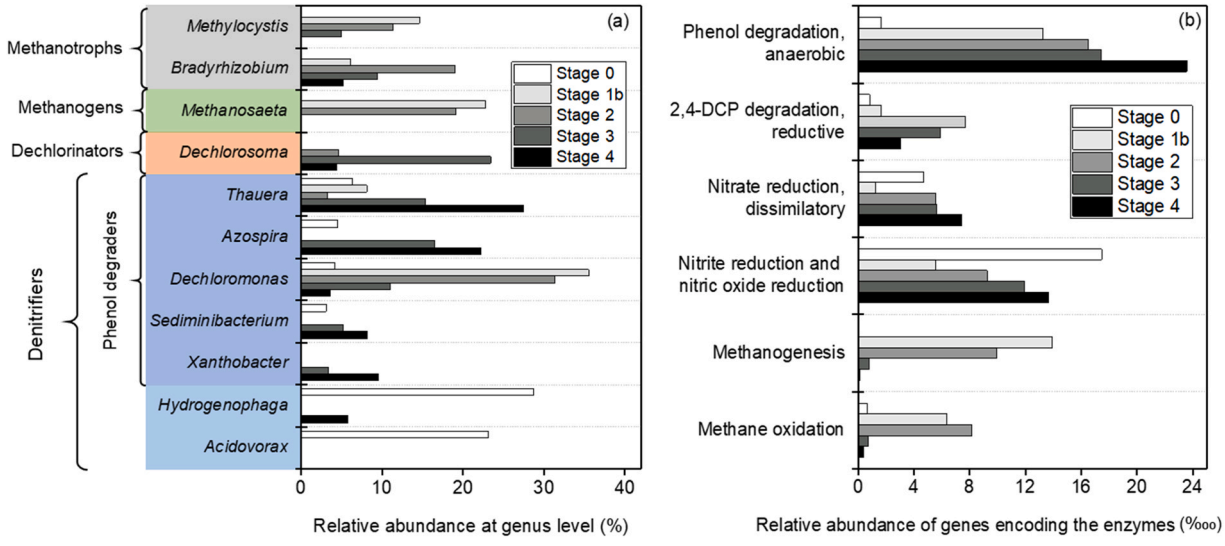

Fig. 3. Phylogenetic profiling of the biofilms at the genus levels, < 3% phylotypes in the Pd^0-biofilms are not shown (a). Relative abundance of predicted functional genes involved in metabolisms of phenol in biofilms by PICRUSt analysis (b).

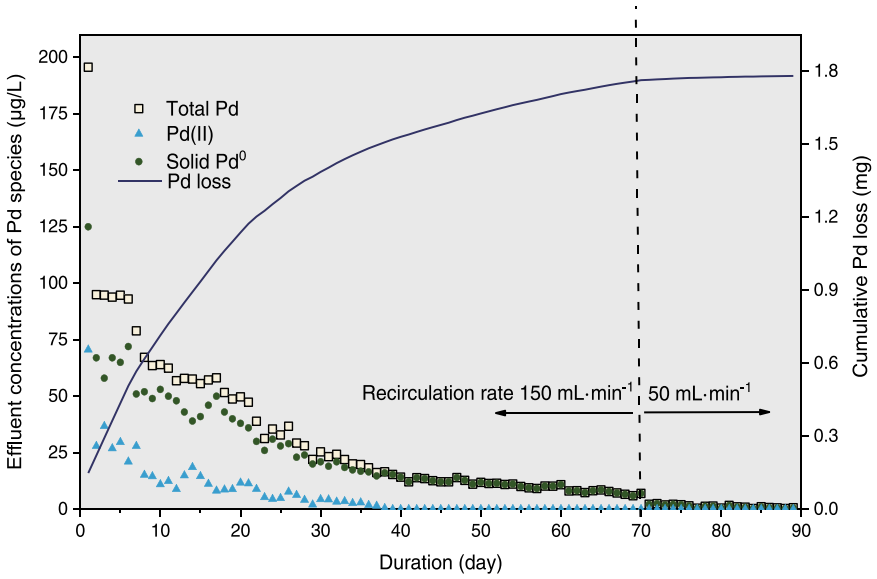

Fig. 4. The effluent concentrations of total Pd, soluble Pd(II), and solid Pd^0, as well as cumulative Pd loss during continuous operation.

adsorption energies on the Pd (1 1 1) plane ($\triangle E_{ads}$, − 1.72 eV for NO_2^- (Shin et al., 2014), − 0.85 eV for 2,4-DCP (Jiang et al., 2018), and − 0.72 eV for 4-CP (Jin, 2010)), NO_2^- possess a much greater affinity for the Pd^0 surface compared to 2,4-DCP or MCP. Therefore, the higher residual NO_2^- concentrations intensified competitive adsorption, which promoted desorption of CPs without further dechlorination.

3.2. Characterizations of microbial communities and functional genes

To understand what bacteria and metabolic pathway were involved with phenol mineralization, we analyzed phylogenetic relationships and predicted metagenomic functions of the microbial communities in the Pd^0-biofilms and biofilm across the stages. Fig. 3 presents the relative microbial abundances and the predicted metagenomic functions reconstructed from the PICRUSt results for the biofilm samples. Table S3 lists the enzymes predicted by metagenomic analysis and involved in phenol degradation.

3.2.1. Microbes involved in phenol fermentation and methane metabolism

When inputs of NO_3^- were zero or small (Stages 1b and 2), the microbial community was dominated by *Dechloromonas*, *Methanosaeta*, *Methylocystis*, and *Bradyrhizobium*. *Dechloromonas* is capable of anaerobic phenol biodegradation via benzoyl-CoA pathway, with acetate being a catabolic product by fermentation (Coates et al., 2002, 2001). *Methanosaeta*, a genus affiliated within *Methanosaetaceae*, utilizes acetate for methanogenesis (Smith and Ingram-Smith, 2007). Seeing *Dechloromonas* and *Methanosaeta* in Stages 1b and 2 points to phenol having been fermented to acetate by *Dechloromonas*, while acetate was utilized to produce CH_4 and CO_2 by *Methanosaeta*. *Methylocystis* is a type II methanotroph (Dedysh and Dunfield, 2011), and *Bradyrhizobium* was also reported to mediate CH_4 oxidation and N_2 fixation (Bao et al., 2014). The small inputs of O_2 may have allowed them to exist in the biofilm via methane oxidation.

3.2.2. Heterotrophic denitrifiers responsible for phenol biodegradation and denitrification

With increased NO_3^- loadings in Stage 3 and 4, methanogens and methanogenesis disappeared, since NO_3^- was amply present as an electron acceptor. Acetate and CH_4 were also absent in the effluent (Fig. S4). The lack of methanogenesis also led to the loss of methane oxidizers.

The relative abundances of *Thauera* (27.4%) and *Azospira* (22.2%) significantly increased after NO_3^- was increased, and they dominated the microbial community by Stage 4. These two genera are heterotrophic denitrifiers that can completely mineralize phenol to CO_2 in the absence of O_2 (Kazuo et al., 2009; Schie and Young, 1998). In contrast, several denitrifying genera capable of utilizing H_2 were enriched in the biofilm fed with NO_3^- only (Stage 0): *Hydrogenophaga* (Park et al., 2005) (28.7%) and *Acidovorax* (Rosenberg, 2013) (23.1%), but become less important in Stage 4 (5.8%). The heterotrophic bacteria could dominate because reductive dechlorination of 2,4-DCP generated their organic electron donor, phenol. The calculated f_s value of denitrification consuming phenol (0.65) is much greater than that of autotrophic denitrification (0.2), which means that heterotrophic denitrification with phenol as a donor has a higher biomass yield and specific growth rate than does autotrophic denitrification using H_2 (Rittmann and McCarty, 2020).

3.2.3. Anaerobic phenol biodegradation through benzoate-CoA pathway

Fig. 3b presents the total abundance of genes for these enzyme-based functions (from Table S3) in the Pd^0-biofilms (Stages 1–4), compared to the denitrifying biofilm alone (Stage 0). In the Pd^0-biofilms fed with 2,4-DCP (Stages 1–4), the PICRUSt-predicted genes encoding anaerobic phenol activation to benzoate-CoA were abundant, while the genes encoding monooxygenases used for aerobic activation through the monooxygenation pathway (Liu et al., 2018) were absent (Table S3). According to the anaerobic metabolic pathway (shown in Fig. S5), the ultimate fate of the benzoate-CoA is to be converted by β-oxidation into acetyl-CoA, which can be oxidized to CO_2 through the tricarboxylic acid (TCA) cycle or be used in acetate production if electron donors are limited (Yang et al., 2021; Holmes et al., 2012). When NO_3^- was absent or limited (Stage 1b and 2), the enrichment of genes encoding methanogenesis and methane oxidation correlated to the higher abundance of genera *Methanosaeta* and *Methylocystis/Bradyrhizobium*, respectively (Fig. 3b). In Stage 3–4, higher NO_3^- loading led to a loss of genes involved with methane metabolism, but stimulated genes responsible NO_3^- reduction.

3.3. Fate of Pd^0NPs associated with the biofilm

Daily monitoring of effluent Pd (Fig. 4) during Stage 1 showed that the loss of solid Pd^0 was larger than loss by Pd(II) leaching. The presence of only detached Pd^0 in effluent (7.2 ± 0.6 μg L^{-1}) at the steady state of Stage 1b suggests that efficient H_2-transfer to the Pd^0NPs prevented oxidation to Pd(II) over the long-term (Luo et al., 2021). To verify that detachment was the major cause of Pd^0 loss, we lowered the

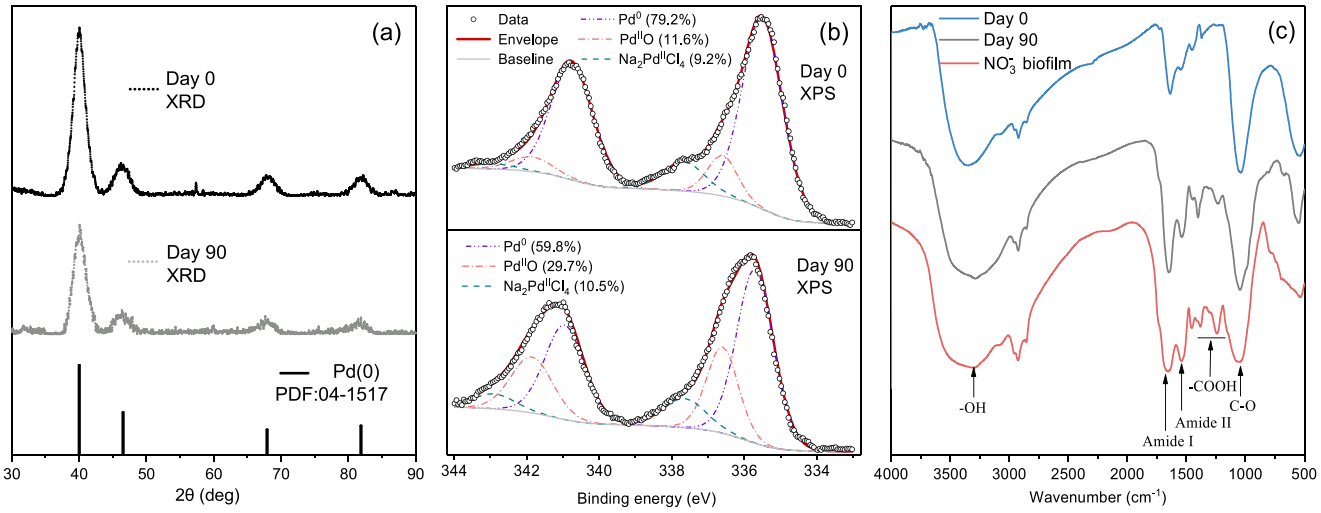

Fig. 5. XRD spectra (a), deconvoluted Pd 3d XPS spectra (b), and FTIR spectra (c) of the solid samples collected at day 0 and day 90, respectively. % values shown in (b) indicate the atomic percentages of various Pd species in each sample.

recirculation rate from 150 to 50 mL min^{-1} at the start of Stage 1c; lowering the recirculation rate decreased the shear stress on the Pd^0NPs on the membranes, and the effluent Pd^0 declined to 0.8 ± 0.4 μg L^{-1}.

The cumulative Pd loss during the 90-day operation (1100 HRTs) was 1.8 mg, only 5.7% of the total Pd^0 deposited in the Pd-MBfR. The low Pd^0 loss rate was close to the 4–8% loss rate reported by Long et al. (2021) and Luo et al. (2021) for *in situ* deposition in H_2-based membrane catalyst-film reactor (MCfRs).

TEM data in Fig. S6 and Fig. S7 characterize the location, morphology, and size of biogenic Pd^0NPs associated with biofilms that were sampled at days 0 and 90. The majority of freshly formed Pd^0NPs located on cell walls and/or in periplasmic spaces (Fig. S6a), because the hydrogenases responsible for enzymatic Pd reduction being associated with the bacterial cells (Mikheenko et al., 2008; Deplanche et al., 2010). After the 90-day operation, Pd^0NPs redispersed more in the extracellular polymeric substance (EPS) matrix (Fig. S6b), and the average size of Pd^0 crystallites moderately decreased from 5.5 ± 1.8–4.6 ± 1.3 nm and with a narrower size distribution (Fig. S7). The XRD spectra in Fig. 5a feature the distinct reflections of crystalline metallic Pd^0, and the estimated average sizes of the Pd^0 crystallites on day 0 and day 90 were 5.0 and 3.8 nm, respectively, similar to the statistical results from the TEM images.

The negative charged EPS matrix helps immobilize the Pd^0NPs via electrostatic stabilization (Zhou et al., 2016b). The XPS spectra (Fig. 5b) displays the PdO content on the Pd^0NPs surfaces in Pd^0-biofilm collected at day 90 (29.7%) was more than at day 0 (11.6%). The PdO was derived from interactions between Pd^0NPs and EPS, and this was confirmed by the FTIR spectra (Fig. 5c). The spectra of the denitrifying biofilm displayed clear peaks at 3300 cm^{-1}, 1550 cm^{-1}, 1255 cm^{-1}, which are attributed to stretching of C-O in carboxylic acid, γNH/γC═O combination in amide II, and O-H in carboxylic groups, respectively. The characteristic peaks of these functional groups became insignificant or disappeared in the Pd^0-biofilm collected at day 0, while these peaks re-emerged in the Pd^0-biofilm after 90-day operation with continued biofilm growth, which supports that the functional groups responsible for Pd immobilization were hydroxyl, carboxyl, and amide groups present in protein and polysaccharides in the EPS. These results are consistent with Sheny et al. (2012), who found the formation of a protein layer bonded on the surface of Pd^0NPs through carboxyl groups after Pd(II) reduction by plant extracts.

4. Conclusion

In the Pd-MBfR, *in-situ* generated Pd^0NPs associated with the biofilm to form a Pd^0-biofilm that provided simultaneous removal of 2,4-DCP and NO_3^-. The Pd^0NPs were well-stabilized and retained by the biofilm, with only 5.7% Pd was lost over 90 days of continuous operation. The Pd-MBfR efficiently hydrodechlorinated 2,4-DCP to phenol, which was fermented via acetogenesis and methanogenesis when influent NO_3^- was minor. Fermentation was suppressed by higher NO_3^- loadings, and phenol was utilized as a more favorable electron donor than H_2 for denitrification and completely mineralized to CO_2. The highest NO_3^- loading slightly inhibited catalytic dechlorination, because the majority of influent NO_3^- was respired by heterotrophic denitrifiers, leaving some NO_2^- reduced by Pd^0 catalysis. The removal of 2,4-DCP was depressed by a high NO_2^- loading that led to unreduced NO_2^- remained in the effluent, and product selectivity toward phenol also declined in parallel. This work demonstrates a promising technology for simultaneously ameliorating co-contamination of NO_3^- and chlorinated phenols, and it provides mechanistic insights into what control denitrification kinetics and DOC removal.

CRediT authorship contribution statement

Chengyang Wu: Conceptualization, Methodology, Formal analysis, Investigation, Resources, Data curation, Writing – original draft, Writing – review & editing, Visualization. **Luman Zhou**: Validation, Formal analysis, Investigation, Data curation, Writing – original draft. **Chen Zhou**: Conceptualization, Methodology, Writing – review & editing. **Yun Zhou**: Writing – review & editing. **Siqing Xia**: Validation, Writing – review & editing, Supervision, Project administration, Funding acquisition. **Bruce E. Rittmann**: Methodology, Writing – review & editing, Supervision.

Declaration of Competing Interest

The authors declare that they have no known competing financial interests or personal relationships that could have appeared to influence the work reported in this paper.

Acknowledgements

This work is supported by Shanghai Leading Talent Project (Grant No. 070) and National Natural Science Foundation of China (Grant No. NSFC 51678422).

Appendix A. Supporting information

Supplementary data associated with this article can be found in the online version at doi:10.1016/j.jhazmat.2021.126916.

References

Addiscott, T.M., Benjamin, N., 2004. Nitrate and human health. Soil Use Manag. 20 (2), 98–104. https://doi.org/10.1111/j.1475-2743.2004.tb00344.x.

Al Bahri, M., Calvo, L., Gilarranz, M.A., Rodriguez, J.J., Epron, F., 2013. Activated carbon supported metal catalysts for reduction of nitrate in water with high selectivity towards N_2. Appl. Catal. B Environ. 138–139, 141–148. https://doi.org/10.1016/j.apcatb.2013.02.048.

Bao, Z., Okubo, T., Kubota, K., Kasahara, Y., Tsurumaru, H., Anda, M., Ikeda, S., Minamisawa, K., 2014. Metaproteomic identification of diazotrophic methanotrophs and their localization in root tissues of field-grown rice plants. Appl. Environ. Microbiol. 80 (16), 5043–5052. https://doi.org/10.1128/AEM.00969-14.

Büchel, K.H., 1984. Political, economic, and philosophical aspects of pesticide use for human welfare. Regul. Toxicol. Pharmacol. 4 (2), 174–191. https://doi.org/10.1016/B978-0-08-029222-9.50006-8.

Cantillo, D., Kappe, C.O., 2014. Immobilized transition metals as catalysts for cross-couplings in continuous flow—a critical assessment of the reaction mechanism and metal leaching. ChemCatChem 6 (12), 3286–3305. https://doi.org/10.1002/cctc.201402483.

Caporaso, J.G., Kuczynski, J., Stombaugh, J., Bittinger, K., Bushman, F.D., Costello, E.K., Fierer, N., Peña, A.G., Goodrich, J.K., Gordon, J.I., Huttley, G.A., Kelley, S.T., Knights, D., Koenig, J.E., Ley, R.E., Lozupone, C.A., McDonald, D., Muegge, B.D., Pirrung, M., Reeder, J., Sevinsky, J.R., Turnbaugh, P.J., Walters, W.A., Widmann, J., Yatsunenko, T., Zaneveld, J., Knight, R., 2010. QIIME allows analysis of high-throughput community sequencing data. Nat. Methods 7, 335–336. https://doi.org/10.1038/nmeth.f.303.

Chaplin, B.P., Reinhard, M., Schneider, W.F., Schüth, C., Shapley, J.R., Strathmann, T.J., Werth, C.J., 2012. Critical review of Pd-based catalytic treatment of priority contaminants in water. Environ. Sci. Technol. 46 (7), 3655–3670. https://doi.org/10.1021/es204087q.

Coates, J.D., Chakraborty, R., Lack, J.G., O'Connor, S.M., Cole, K.A., Bender, K.S., Achenbach, L.A., 2001. Anaerobic benzene oxidation coupled to nitrate reduction in pure culture by two strains of Dechloromonas. Nature 411 (6841), 1039–1043. https://doi.org/10.1038/35082545.

Coates, J.D., Chakraborty, R., McInerney, M.J., 2002. Anaerobic benzene biodegradation—a new era. Res. Microbiol. 153 (10), 621–628. https://doi.org/10.1016/S0923-2508(02)01378-5.

Dedysh, S.N., Dunfield, P.F., 2011. Chapter three - Facultative and obligate methanotrophs: how to identify and differentiate them. Methods Enzymol. 495, 31–44. https://doi.org/10.1016/B978-0-12-386905-0.00003-6.

Deplanche, K., Caldelari, I., Mikheenko, I.P., Sargent, F., Macaskie, L.E., 2010. Involvement of hydrogenases in the formation of highly catalytic Pd(0) nanoparticles by bioreduction of Pd(II) using Escherichia coli mutant strains. Microbiology 156 (9), 2630–2640. https://doi.org/10.1099/mic.0.036681-0.

Estevinho, B.N., Martins, I., Ratola, N., Alves, A., Santos, L., 2007. Removal of 2,4-dichlorophenol and pentachlorophenol from waters by sorption using coal fly ash from a Portuguese thermal power plant. J. Hazard. Mater. 143 (1–2), 535–540. https://doi.org/10.1016/j.jhazmat.2006.09.072.

Gao, J., Liu, L., Liu, X., Zhou, H., Huang, S., Wang, Z., 2008. Levels and spatial distribution of chlorophenols – 2,4-dichlorophenol, 2,4,6-trichlorophenol, and pentachlorophenol in surface water of China. Chemosphere 71 (6), 1181–1187. https://doi.org/10.1016/j.chemosphere.2007.10.018.

Gonzalez, M., Miglioranza, K.S.B., Shimabukuro, V.M., Quiroz Londoño, O.M., Martinez, D.E., Aizpún, J.E., Moreno, V.J., 2012. Surface and groundwater pollution by organochlorine compounds in a typical soybean system from the south Pampa, Argentina. Environ. Earth Sci. 65 (2), 481–491. https://doi.org/10.1007/s12665-011-1328-x.

Greco, R., Goessler, W., Cantillo, D., Kappe, C.O., 2015. Benchmarking immobilized di- and triarylphosphine palladium catalysts for continuous-flow cross-coupling reactions: efficiency, durability, and metal leaching studies. ACS Catal. 5 (2), 1303–1312. https://doi.org/10.1021/cs5020089.

Holmes, D.E., Risso, C., Smith, J.A., Lovley, D.R., 2012. Genome-scale analysis of anaerobic benzoate and phenol metabolism in the hyperthermophilic archaeon Ferroglobus placidus. ISME J. 6 (1), 146–157. https://doi.org/10.1038/ismej.2011.88.

House, W.A., Leach, D., Long, J.L.A., Cranwell, P., Smith, C., Bharwaj, L., Meharg, A., Ryland, G., Orr, D.O., Wright, J., 1997. Micro-organic compounds in the Humber rivers. Sci. Total Environ. 194–195, 357–371. https://doi.org/10.1016/S0048-9697(96)05375-2.

Jiang, G., Wang, K., Li, J., Fu, W., Zhang, Z., Johnson, G., Lv, X., Zhang, Y., Zhang, S., Dong, F., 2018. Electrocatalytic hydrodechlorination of 2,4-dichlorophenol over palladium nanoparticles and its pH-mediated tug-of-war with hydrogen evolution. Chem. Eng. J. 348, 26–34. https://doi.org/10.1016/j.cej.2018.04.173.

Jin, Z., 2010. Study on the Preparation of Supported Pd Catalyst and Their Catalytic Activity for Hydrodechlorination and Reductive Alkylation (Doctoral dissertation). East China University of Science and Technology, Shanghai.

Kazuo, S., Hiroyasu, S., Motoharu, O., Takashi, M., 2009. Microorganisms involved in anaerobic phenol degradation in the treatment of synthetic coke-oven wastewater detected by RNA stable-isotope probing. FEMS Microbiol. Lett. 291 (2), 169–174. https://doi.org/10.1111/j.1574-6968.2008.01448.x.

Langille, M.G.I., Zaneveld, J., Caporaso, J.G., McDonald, D., Knights, D., Reyes, J.A., Clemente, J.C., Burkepile, D.E., Vega Thurber, R.L., Knight, R., Beiko, R.G., Huttenhower, C., 2013. Predictive functional profiling of microbial communities using 16S rRNA marker gene sequences. Nat. Biotechnol. 31 (9), 814–821. https://doi.org/10.1038/nbt.2676.

Laspidou, C.S., Rittmann, B.E., 2002. A unified theory for extracellular polymeric substances, soluble microbial products, and active and inert biomass. Water Res. 36 (11), 2711–2720. https://doi.org/10.1016/S0043-1354(01)00413-4.

Lee, K.-C., Rittmann, B.E., 2002. Applying a novel autohydrogenotrophic hollow-fiber membrane biofilm reactor for denitrification of drinking water. Water Res. 36 (8), 2040–2052. https://doi.org/10.1016/j.watres.2020.116465.

Liu, X., Chen, L., Yang, M., Tan, C., Chu, W., 2020. The occurrence, characteristics, transformation and control of aromatic disinfection by-products: a review. Water Res. 184, 116076 https://doi.org/10.1016/j.watres.2020.116076.

Liu, J., Zhang, X., 2014. Comparative toxicity of new halophenolic DBPs in chlorinated saline wastewater effluents against a marine alga: halophenolic DBPs are generally more toxic than haloaliphatic ones. Water Res. 65, 64–72. https://doi.org/10.1016/j.watres.2014.07.024.

Liu, Z., Zhou, C., Ontiveros-Valencia, A., Luo, Y.-H., Long, M., Xu, H., Rittmann, B.E., 2018. Accurate O_2 delivery enabled benzene biodegradation through aerobic activation followed by denitrification-coupled mineralization. Biotechnol. Bioeng. 115 (8), 1988–1999. https://doi.org/10.1002/bit.26712.

Li, Z., Yang, S., Inoue, Y., Yoshida, N., Katayama, A., 2010. Complete anaerobic mineralization of pentachlorophenol (PCP) under continuous flow conditions by sequential combination of PCP-dechlorinating and phenol-degrading consortia. Biotechnol. Bioeng. 107 (5), 775–785. https://doi.org/10.1002/bit.22841.

Long, M., Ilhan, Z.E., Xia, S., Zhou, C., Rittmann, B.E., 2018. Complete dechlorination and mineralization of pentachlorophenol (PCP) in a hydrogen-based membrane biofilm reactor (MBfR). Water Res. 144, 134–144. https://doi.org/10.1016/j.watres.2018.06.071.

Long, M., Long, X., Zheng, C.-W., Luo, Y.-H., Zhou, C., Rittmann, B.E., 2021. Para-chlorophenol (4-CP) removal by a palladium-coated biofilm: coupling catalytic dechlorination and microbial mineralization via denitrification. Environ. Sci. Technol. 55, 6309–6319. https://doi.org/10.1021/acs.est.0c08307.

Long, M., Zeng, C., Wang, Z., Xia, S., Zhou, C., 2020. Complete dechlorination and mineralization of para-chlorophenol (4-CP) in a hydrogen-based membrane biofilm reactor (MBfR). J. Clean. Prod. 276, 123257 https://doi.org/10.1016/j.jclepro.2020.123257.

Long, M., Zhou, C., Xia, S., Guadiea, A., 2017. Concomitant Cr(VI) reduction and Cr(III) precipitation with nitrate in a methane/oxygen-based membrane biofilm reactor. Chem. Eng. J. 315, 58–66. https://doi.org/10.1016/j.cej.2017.01.018.

Luo, Y.-H., Zhou, C., Bi, Y., Long, X., Wang, B., Tang, Y., Krajmalnik-Brown, R., Rittmann, B.E., 2021. Long-term continuous co-reduction of 1,1,1-trichloroethane and trichloroethene over palladium nanoparticles spontaneously deposited on H_2-transfer membranes. Environ. Sci. Technol. 55 (3), 2057–2066. https://doi.org/10.1021/acs.est.0c05217.

Mikheenko, I.P., Rousset, M., Dementin, S., Macaskie, L.E., 2008. Bioaccumulation of palladium by Desulfovibrio fructosivorans wild-type and hydrogenase-deficient strains. Appl. Environ. Microbiol. 74 (19), 6144–6146. https://doi.org/10.1128/AEM.02538-07.

Park, H.I., Choi, Y.J., Pak, D., 2005. Autohydrogenotrophic denitrifying microbial community in a glass beads biofilm reactor. Biotechnol. Lett. 27 (13), 949–953. https://doi.org/10.1007/s10529-005-7654-x.

Qiu, Y.-L., Hanada, S., Ohashi, A., Harada, H., Kamagata, Y., Sekiguchi, Y., 2008. Syntrophorhabdus aromaticivorans gen. nov., sp. nov., the first cultured anaerobe capable of degrading phenol to acetate in obligate syntrophic associations with a hydrogenotrophic methanogen. Appl. Environ. Microbiol. 74 (7), 2051–2058. https://doi.org/10.1128/AEM.02378-07.

Rittmann, B.E., McCarty, P.L., 2020. Environmental Biotechnology: Principles and Applications, second ed. McGraw-Hill Book Co, New York.

Rosenberg, E., 2013. The Prokaryotes: Alphaproteobacteria and Betaproteobacteria. Springer, Heidelberg.

Schie, P., Young, L.Y., 1998. Isolation and characterization of phenol-degrading denitrifying bacteria. Appl. Environ. Microbiol. 64 (7), 2432–2438. https://doi.org/10.1128/AEM.64.7.2432-2438.1998.

Sheny, D.S., Philip, D., Mathew, J., 2012. Rapid green synthesis of palladium nanoparticles using the dried leaf of Anacardium occidentale. Spectrochim. Acta Part A Mol. Biomol. Spectrosc. 91, 35–38. https://doi.org/10.1016/j.saa.2012.01.063.

Shin, H., Jung, S., Bae, S., Lee, W., Kim, H., 2014. Nitrite reduction mechanism on a Pd surface. Environ. Sci. Technol. 48 (21), 12768–12774. https://doi.org/10.1021/es503772x.

Smith, K.S., Ingram-Smith, C., 2007. Methanosaeta, the forgotten methanogen? Trends Microbiol. 15 (4), 150–155. https://doi.org/10.1016/j.tim.2007.02.002.

Tang, W.Z., Huang, C.P., 1996. 2,4-Dichlorophenol oxidation kinetics by Fenton's reagent. Environ. Technol. 17 (12), 1371–1378. https://doi.org/10.1080/09593330.1996.9618465.

Tang, Y., Zhou, C., Van Ginkel, S.W., Ontiveros-Valencia, A., Shin, J., Rittmann, B.E., 2012. Hydrogen permeability of the hollow fibers used in H_2-based membrane biofilm reactors. J. Membr. Sci. 407–408, 176–183. https://doi.org/10.1016/j.memsci.2012.03.040.

United States Environmental Protection Agency, 2012. Drinking Water Standards and Health Advisories, Office of Water, U.S. EPA, Washington, D.C., EPA 822-B-00-001.

Wang, X., Xing, L., Qiu, T., Han, M., 2013. Simultaneous removal of nitrate and pentachlorophenol from simulated groundwater using a biodenitrification reactor

packed with corncob. Environ. Sci. Pollut. Res. 20 (4), 2236–2243. https://doi.org/10.1007/s11356-012-1092-9.

Weigel, J., Zhang, X., Dalton, D., Kohring, G.-W., 1990. Degradation of 2,4-dichlorophenol in anaerobic freshwater lake sediments, emerging technologies in hazardous. Waste Manag. 422, 119–141. https://doi.org/10.1021/bk-1990-0422.ch008.

Wu, C., Zhou, L., Zhou, Y., Zhou, C., Xia, S., Rittmann, B.E., 2021. Dechlorination of 2,4-dichlorophenol in a hydrogen-based membrane palladium-film reactor: performance, mechanisms, and model development. Water Res. 188, 116465 https://doi.org/10.1016/j.watres.2020.116465.

Xia, S., Xu, X., Zhou, C., Wang, C., Zhou, L., Rittmann, B.E., 2016. Direct delivery of CO_2 into a hydrogen-based membrane biofilm reactor and model development. Chem. Eng. J. 290, 154–160. https://doi.org/10.1016/j.cej.2016.01.021.

Xia, S., Zhang, Z., Zhong, F., Zhang, J., 2011. High efficiency removal of 2-chlorophenol from drinking water by a hydrogen-based polyvinyl chloride membrane biofilm reactor. J. Hazard. Mater. 186 (2), 1367–1373. https://doi.org/10.1016/j.jhazmat.2010.12.023.

Xie, W., Wang, F., Guo, L., Chen, Z., Sievert, S.M., Meng, J., Huang, G., Li, Y., Yan, Q., Wu, S., Wang, X., Chen, S., He, G., Xiao, X., Xu, A., 2011. Comparative metagenomics of microbial communities inhabiting deep-sea hydrothermal vent chimneys with contrasting chemistries. ISME J. 5 (3), 414–426. https://doi.org/10.1038/ismej.2010.144.

Yang, K., Zhao, Y., Ji, M., Li, Z., Zhai, S., Zhou, X., Wang, Q., Wang, C., Liang, B., 2021. Challenges and opportunities for the biodegradation of chlorophenols: aerobic, anaerobic and bioelectrochemical processes. Water Res. 193, 116862 https://doi.org/10.1016/j.watres.2021.116862.

Zhang, J.F., Liu, H., Sun, Y.Y., Wang, X.R., Wu, J.C., Xue, Y.Q., 2005. Responses of the antioxidant defenses of the Goldfish Carassius auratus, exposed to 2,4-dichlorophenol. Environ. Toxicol. Pharmacol. 19 (1), 185–190. https://doi.org/10.1016/j.etap.2004.07.001.

Zhang, T., Tremblay, P.-L., Chaurasia, A.K., Smith, J.A., Bain, T.S., Lovely, D.R., 2013. Anaerobic benzene oxidation via phenol in Geobacter metallireducens. Appl. Environ. Microbiol. 79 (24), 7800–7806. https://doi.org/10.1128/AEM.03134-13.

Zhou, C., Ontiveros-Valencia, A., Nerenberg, R., Tang, Y., Friese, D., Krajmalnik-Brown, R., Rittmann, B.E., 2018. Hydrogenotrophic microbial reduction of oxyanions with the membrane biofilm. Front. Microbiol. 9, 3268. https://doi.org/10.3389/fmicb.2018.03268.

Zhou, C., Ontiveros-Valencia, A., Wang, Z., Maldonado, J., Zhao, H.-P., Krajmalnik-Brown, R., Rittmann, B.E., 2016a. Palladium recovery in a H_2-based membrane biofilm reactor: formation of Pd(0) nanoparticles through enzymatic and autocatalytic reductions. Environ. Sci. Technol. 50 (5), 2546–2555. https://doi.org/10.1021/acs.est.5b05318.

Zhou, C., Wang, Z., Marcus, A.K., Rittmann, B.E., 2016b. Biofilm-enhanced continuous synthesis and stabilization of palladium nanoparticles (PdNPs). Environ. Sci. Nano 3 (6), 1396–1404. https://doi.org/10.1039/c6en00308g.

Zhou, C., Wang, Z., Ontiveros-Valencia, A., Long, M., Lai, C.-y, Zhao, H.-p, Xia, S., Rittmann, B.E., 2017. Coupling of Pd nanoparticles and denitrifying biofilm promotes H_2-based nitrate removal with greater selectivity towards N_2. Appl. Catal. B Environ. 206, 461–470. https://doi.org/10.1016/j.apcatb.2017.01.068.